

# Construction of the Numerical Wave Databases Anemoc-2 on the Mediterranean Sea and the Atlantic Ocean Through Hindcast Simulations Over the Period 1979–2010

Anne-Laure Tiberi-Wadier, Amélie Laugel and Michel Benoit

## 1 Introduction

From 2003 to 2007, CEREMA (Centre for expertise and engineering on risks, urban, and country planning, environment, and mobility, Brest, France) and EDF R&D LNHE (National Hydraulic and Environment Laboratory, Chatou, France) have been collaborating to build two continuous wave databases through numerical hindcast simulations. The first one covers the North-East part of the Atlantic Ocean, the English Channel, and the North Sea [2, 3]. The second one covers the Mediterranean Sea [12, 13].

These first versions of the databases, called ANEMOC, for “Atlas Numérique d’Etats de Mer Océanique et Côtier” (i.e. Numerical Atlas of Oceanic and Coastal Sea States), are available through Internet since 2008 (see: <http://anemoc.cetmef.developpement-durable.gouv.fr/>). Wave climate analyses were performed based on the simulated time series (distributions of individual sea-state parameters, seasonal effects, estimation of extreme values, etc.). These data have been used in a number of research projects and engineering studies.

In order to ameliorate these results, and complementary to other wave databases [5, 6], from 2010 to 2013, these institutes continued their collaboration, through the

---

A.-L. Tiberi-Wadier (✉)

Centre D’Étude et D’expertise Sur Les Risques, La Mobilité et L’Aménagement (CEREMA),  
155 Rue Pierre Bouguer, BP 5, 29280 Plouzané Cédex, France  
e-mail: Anne-Laure.Tiberi-Wadier@cerema.fr

A. Laugel · M. Benoit

Laboratoire D’Hydraulique Saint Venant (CEREMA, EDF R&D, ENPC),  
6 Quai Watier, BP 49, 78401 Chatou, France  
e-mail: Amelie.Laugel@edf.fr

M. Benoit

e-mail: Michel.Benoit@edf.fr

Saint-Venant Laboratory, in order to create new versions of these wave databases called ANEMOC-2. Following improvements have been made:

- i. The Atlantic model covers a larger area: main parts of the Atlantic Ocean, from 63°S to 80°N;
- ii. The temporal coverage of the atlases is larger: 32 years, from 1979 to 2010;
- iii. Wave spectrum discretization is finer: 36 directions and 32 frequencies (from 0.0345 to 0.66 Hz, corresponding to periods from 1.5 to 29 s);
- iv. The resolution of the wind field used for forcing the wave model is finer in time and space: 1 h and  $0.312^\circ \times 0.312^\circ$  resolution;
- v. The computational grids are refined: resolution of about 800 m to 1 km along the French coasts.

This article presents the construction of the wave models ANEMOC-2 and their associated results. The methodology is described, focusing with more details and results on the Mediterranean model of ANEMOC-2, then results of both Mediterranean Sea and Atlantic Ocean atlases are expressed. Section 2 presents the setup of the models and wind data used as forcing. Section 3 is devoted to the calibration step using altimetry data, and highlights the accuracy of the wave model ANEMOC-2 compared to satellite measurements. In Sect. 4, comparisons of the wave simulations with buoy measurements are achieved, first for the validation step and then focusing on particular storm events. Finally, conclusion and perspectives are exposed in Sect. 5.

## 2 Setup of the Wave Models

### 2.1 *The Spectral Wave Code TOMAWAC*

The simulations are performed with the numerical wave model TOMAWAC [1], which is a third generation spectral model, solving the wave action density balance equation. TOMAWAC is a module of TELEMAC-MASCARET hydro-informatics suite ([www.opentelemac.org](http://www.opentelemac.org)). It models the evolution in space and time of the directional wave spectrum under unsteady wind forcing. It can take into account the input of energy from the wind, nonlinear wave-wave interactions, dissipation due to white-capping, bottom friction, and depth-induced breaking in shallow water. TOMAWAC is very suitable for coastal modeling applications as the computations are performed on unstructured irregular grids. This allows refining the computational mesh in areas of interest and in case of complex bathymetry and shoreline.

For the present version of ANEMOC-2, tidal and current effects are not taken into account. The models are run with water depths corresponding to the mean tidal level. The wave spectrum is divided into 32 frequencies (from 0.034 to 0.66 Hz, i.e., from 1.5 to 29 s) and 36 directions (constant angular resolution of  $10^\circ$ ). All ANEMOC-2 models have been constructed over 32 years (1979–2010).

Regarding physical processes, the Mediterranean model and the oceanic Atlantic model include the effects of wind input, nonlinear wave-wave interactions, and dissipation due to white-capping. Bottom friction dissipation and dissipation through depth-induced breaking are taken into account for the Atlantic coastal model only.

A set of seven sea state parameters are calculated from the directional spectra and stored on output with a 1-hour resolution: (i) significant wave height, (ii) energetic period, (iii) mean period, (iv) peak period, (v) mean direction, (vi) angular spreading, and (vii) wave power.

## 2.2 The Mediterranean Wave Model

The Mediterranean wave model covers the whole Mediterranean Sea, from 30° to 46° North in latitude, and from 6° West to 37° East in longitude. The size of the mesh is variable. It is about 800 m along the French coasts, from 3 to 8 km along the Spanish and Italian coasts, about 25 km along North Africa coasts and a maximum resolution of 50 km is imposed over the rest of the domain. The mesh is composed of 15,343 nodes and 28,159 elements. Bathymetry data are derived from the Europe base (LEGOS). Figure 1 represents the mesh used in the simulations and the associated mean sea level bathymetry.

No wave spectrum is imposed at the boundaries of this model. We consider that the waves are generated only inside the model due to wind forcing.

The computational time step for this model is 100 s. Each year is simulated independently, starting the simulation on the 22nd of December of the previous year to initialize the model. It takes about 30 h to simulate a whole year by performing a parallel computation on 12 processors.

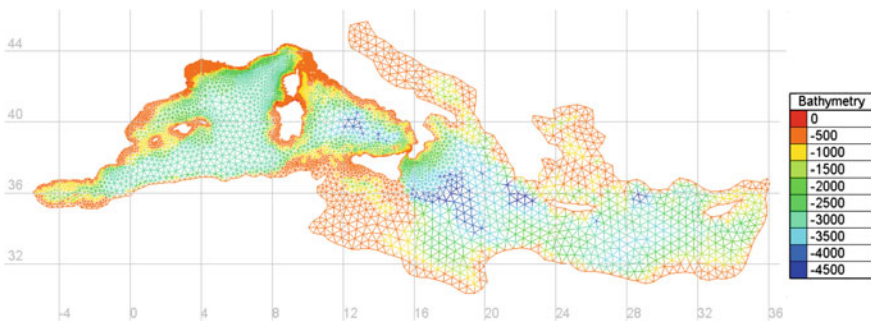


**Fig. 1** Bathymetry, resolution and spatial domain of the Mediterranean model of ANEMOC-2

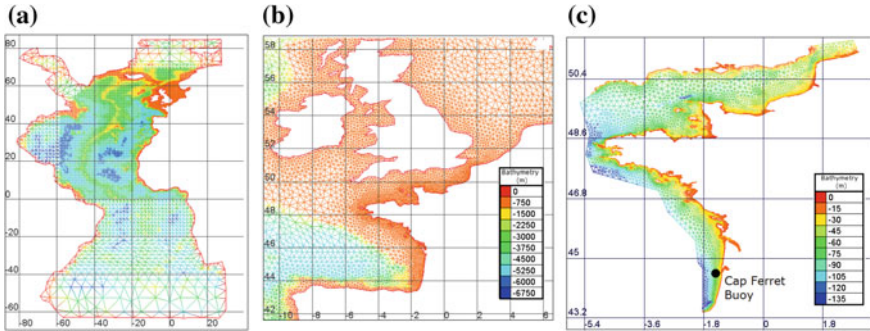


**Fig. 2** Bathymetry, resolution and spatial domains of Oceanic **a**, **b** and Coastal **c** meshes of ANEMOC-2. Black node locates of the Cap Ferret buoy

### 2.3 The Atlantic Wave Models

The Atlantic Ocean is modeled by means of two unstructured nested grids. The first grid covers the Atlantic Ocean (Fig. 2a) from 63°S to 80°N with a resolution of 1.875° in the southern hemisphere, increasing up to 0.6° in the North East Atlantic to finally match with 20 and 10 km resolution along the European and French coasts, respectively (Fig. 2b). This “oceanic” grid provides wave spectra boundary conditions to the second mesh, named “coastal” grid and focusing on the Atlantic, English Channel, and North Sea French coasts (Fig. 2c). The coastal grid covers the English Channel and reaches the UK coast with a resolution of 3 to 4 km. It also covers the Atlantic and North Sea French shoreline from the 100 m depth isobaths and reaches the French coast with a 1 km resolution. Both grids have been constructed at mean sea level using Gebco ([www.gebco.net](http://www.gebco.net)) and Europe (LEGOS) bathymetric databases. The oceanic mesh comprises 13,426 nodes and 22,548 elements, while the coastal one comprises 16,295 nodes and 29,018 elements.

The time steps for the oceanic and coastal models are 300 and 180 s, respectively. One-year simulation lasts about 8 and 12 h for the each model on a 24 processors computer.

### 2.4 Wind Data Used to Force the Models

The wave models are forced with the 10 m wind fields from the Climate Forecast System Reanalysis (CFSR) database [15] from the National Oceanic and Atmospheric Administration (NOAA). Wind components are provided every hour, on a regular grid with resolution of 0.312° over a period of 32 years, from 1979 to

2010. Their high spatial and temporal resolutions promote their use as an alternative to reanalysis with a 6-hour time resolution. Therefore, a better representation of the storm events is expected, in particular regarding the times of the peak of the storms. These wind fields are linearly interpolated on the computational grids shown on Figs. 1 and 2.

### 3 Calibration of the Wave Models

#### 3.1 General Methodology and Data

In the study, the numerical wave models have been calibrated by comparing the results of the simulations with the altimeter measurements from the GlobWave database ([14], [www.globwave.org](http://www.globwave.org)). This database provides altimeter observations of calibrated significant wave height  $H_{m0}$  for a set of eight satellites, over the period 1985–2014.

For the calibration step, simulations results of  $H_{m0}$  are linearly interpolated in space and time on the satellite tracks. Once this collocation step is achieved, two sets of data are considered: the observed series ( $x_i$ ), and the simulated series ( $y_i$ ). To assess and quantify the matching between both, four statistical parameters are calculated, as defined in Table 1. These statistical parameters are computed on various domains with different sizes: the whole computational domain, or sub-domains in areas of interest, or at the scale of cells of  $0.5^\circ \times 0.5^\circ$  or  $1^\circ \times 1^\circ$ .

Several methods have been tested to optimize calibration: (i) test of different combinations of physical laws implemented in TOMAWAC concerning generation, dissipation and energy transfer, (ii) modification of the coefficients in the physical laws, (iii) calibrating wind fields by comparison quantile/quantile with scatterometers measurements, and (iv) adjusting the elevation of the wind imposed in the model.

After comparing these various options, we decided not to modify the wind fields but to select the most accurate physical source and sink terms (option (i) above), and if necessary modifying their default parameters and setting (option (ii) above).

**Table 1** Statistical parameters used to compare series of simulations results ( $y_i$ ) with reference date ( $x_i$ )

Bias	Root mean square error (RMSE)	Scatter index	Symmetric slope
$\frac{1}{n} \sum_1^n (y_i - x_i)$	$\sqrt{\frac{1}{n} \sum_1^n (y_i - x_i)^2}$	$\sqrt{\frac{\sum_1^n (y_i - x_i)^2}{\sum_1^n x_i^2}}$	$\sqrt{\frac{\sum_1^n y_i^2}{\sum_1^n x_i^2}}$

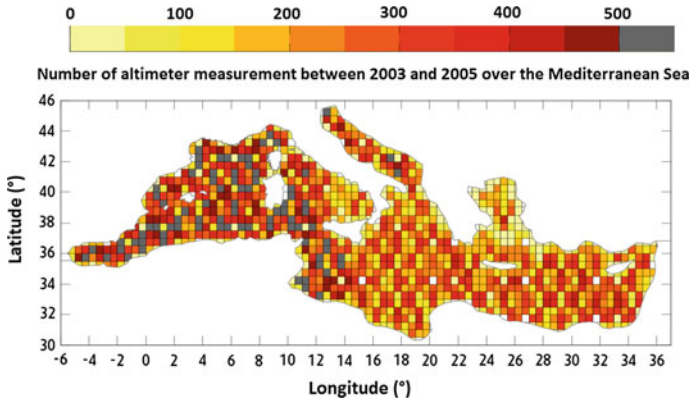


**Fig. 3** Number of altimeter measurements from ENVISAT and ERS-2 between 2003 and 2005 over the Mediterranean Sea

## 3.2 Calibration of the Mediterranean Model

### 3.2.1 Altimeter Data Used for the Calibration

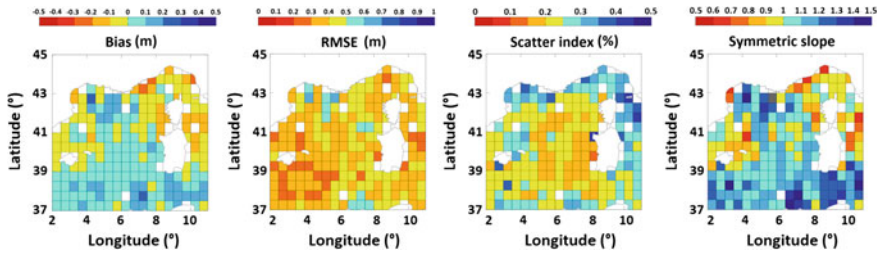
In order to calibrate the Mediterranean wave model, observations of  $H_{m0}$  from satellites Envisat (2002–2012) and ERS-2 (1995–2009) are used. Indeed, these satellites offer a good spatial coverage over the Mediterranean Sea of about 80 km between tracks, with a return period of 35 days.

Figure 3 shows the number of satellite measurements per cells of  $0.5^\circ \times 0.5^\circ$  in size over the Mediterranean Sea during the period 2003–2005. This figure shows that altimeter measurement coverage is dense enough to allow the calculation of statistics, especially on the west Mediterranean area (more than 200/300 measurements over each cell of  $0.5^\circ \times 0.5^\circ$ ).

The selected parameterization of the Mediterranean model ANEMOC-2 corresponds to: (i) Janssen parametrization [9, 10] for the wind-wave induced generation, (ii) Discrete Interaction Approximation [8] for the nonlinear quadruplet interactions and (iii) Komen et al. parameterization [11] for the white-capping dissipation. In this formulation, the dissipation coefficient has been lowered to 3.2 and the weighting coefficient to 0.4. Indeed, the modification of these two coefficients avoids too much underestimation of the wave height.

### 3.2.2 Maps of Statistical Parameters

As results, the plots of Fig. 4 represent the statistical parameters calculated for the significant wave height  $H_{m0}$  between ANEMOC-2 results and the altimeter measurements, on cells of  $0.5^\circ \times 0.5^\circ$  over the period 2003–2005 on the west Mediterranean Sea which is our area of interest.



**Fig. 4** Bias, RMSE, scatter index and symmetric slope between ANEMOC-2  $H_{m0}$  wave height and the altimeters measurements over the period 2003–2005

In comparison with altimeter data, ANEMOC-2 has a negative bias in the area around Corsica, at the East of Marseille and along the Italian and Spanish coast. This means that the wave model slightly underestimates the altimeters observations in these areas. On the contrary, it presents a positive bias in the area of the Lion Gulf and more generally offshore, corresponding to a slight overestimation of  $H_{m0}$  from the wave model. However, ANEMOC-2 results show a bias between  $-10$  and  $10$  cm over a large area, which is quite a good approximation of the observations.

The analysis provided by the other statistical indices corroborates these results. At the South of the Balearics, the root mean square error (RMSE) is between  $25$  and  $30$  cm. It increases and reaches about  $50$  cm near the French coast, and occasionally exceeds  $50$  cm. The scatter index shows a variation similar to that of the RMSE. The statistics are better offshore than in coastal areas. It is about  $10$  to  $25$  % offshore, and reaches  $25$  to  $35$  % near the French coast. The higher values are at the East of Corsica ( $45$  % locally). The values calculated for the symmetric slope are similar to the values of the bias, and so confirm the areas of overestimation and underestimation of the wave atlas.

This difference between offshore and coastal area could be explained by two reasons: (i) the complex orography of the Mediterranean coast involves complications for the simulation of atmospheric forcing in a first time, and then for the simulation of shallow water physical processes in the wave model and (ii) the altimetry observations are biased in the vicinity of the shoreline because of the instrument initialization needed in case of altimeter path from the land to the ocean. Therefore, the validation step provided by means of coastal buoy will help to define the accuracy of ANEMOC-2 in coastal area.

### 3.2.3 Scatter Plots

The comparison between altimeter measurements and simulation wave fields has shown that depending on the areas, the wave model does not offer the same characteristics. Figure 5 represents the scatter plots for simulations wave height and altimeter measurements over the period 2003–2005. Three different areas are considered, which are shown by the plots of Fig. 5a, d, g. Green points represents



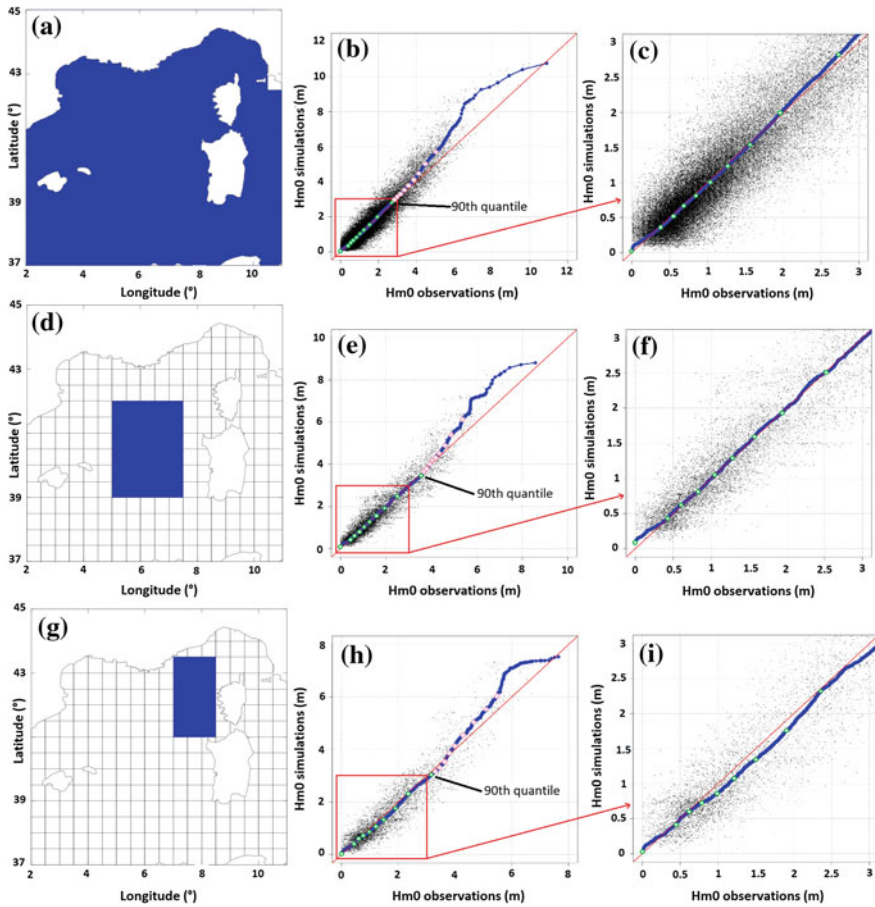


**Fig. 5** Scatter plots of simulations wave height  $H_{m0}$  and altimeter measurements over three areas of the Mediterranean Sea

from the 10th to the 90th percentile and pink points represents from the 91th to the 99th percentile. The 90th percentile is indicated with an arrow. In each line of graphics, the first figure represents the area considered for the calculation (Fig. 5a, d, g), the second one represents the scatter plot for the whole distribution (Fig. 5b, e, h), and the last one (Fig. 5c, f, i) represents a zoom focusing on the waves height inferior to 3 m, corresponding approximately to the 80th or 90th percentile.

In the first area, the scatter plot shows that ANEMOC-2 results are very good up to the 90th percentile. From the 90th to the 95th percentile, we see a moderate overestimation. The overestimation is larger for waves higher than the 95th percentile. The tail of the distribution (values higher than the 99th percentile) is not very well modeled. The overestimation is 3.6 % for the 90th percentile and it is about 13 % for the 99th percentile.



In the second area in which the bias is positive, the scatter plot shows that ANEMOC-2 results are good up to the 96th percentile. For higher values, we see a moderate overestimation. For the 90th percentile, we see 2 % of underestimation. The overestimation is about 14 % for the 99th percentile.

Finally, the third area in which the bias is negative, the scatter plot shows that ANEMOC-2 slightly underestimates the wave values between the 40th and the 93th percentile. For the higher percentiles, we always notice an overestimation, but less than in the second area.

### 3.3 Calibration of the Atlantic Model

The calibration of the Atlantic model was performed over the period 2000–2009 with the GlobWave altimeters [14] from Topex/Poseidon, ERS-2, Geosat Follow On, Envisat, Jason-1, and Jason-2. It allowed to select the best parameterization of TOMAWAC for this oceanic model, which corresponds to the combination of the Janssen model [9, 10] for the wind-wave induced generation, the so-called BAJ parameterization [4] for the white-capping dissipation and the Discrete Interaction Approximation (DIA) for the nonlinear quadruplet interactions [8]. The parameterization of the coastal model is similar for these three physical processing, while dissipation terms from Thornton and Guza [16] and from the JONSWAP campaign [7] are respectively added for the bathymetric breaking and the bottom friction processes.

As a result of the calibration step, Fig. 6 illustrates the bias between the ANEMOC-2  $H_{m0}$  and the six altimeters observations over the period 2007-2009 focusing on the Bay of Biscay and North Sea areas over a grid a  $1^\circ \times 1^\circ$ . Over the North East Atlantic Ocean, the bias varies between  $\pm 10$  cm which corresponds to a quite good reproduction of the  $H_{m0}$ . To be more specific, the bias value is  $-6$  cm in the Bay of Biscay and  $-5$  cm in the North Sea area, corresponding, respectively, to scatter index of 12 and 13 % and to RMSE of 37 and 34 cm. Therefore, this analysis characterizes the slight underestimation of the  $H_{m0}$  from ANEMOC-2 in comparison to the altimeter observations.

## 4 Validation of the Models Against Buoy Data

### 4.1 General Methodology

After the calibration step, the simulation results were validated by comparison with uncorrelated measurements from buoy data. The data sets used here are fully independent from the ones used in the previous section.

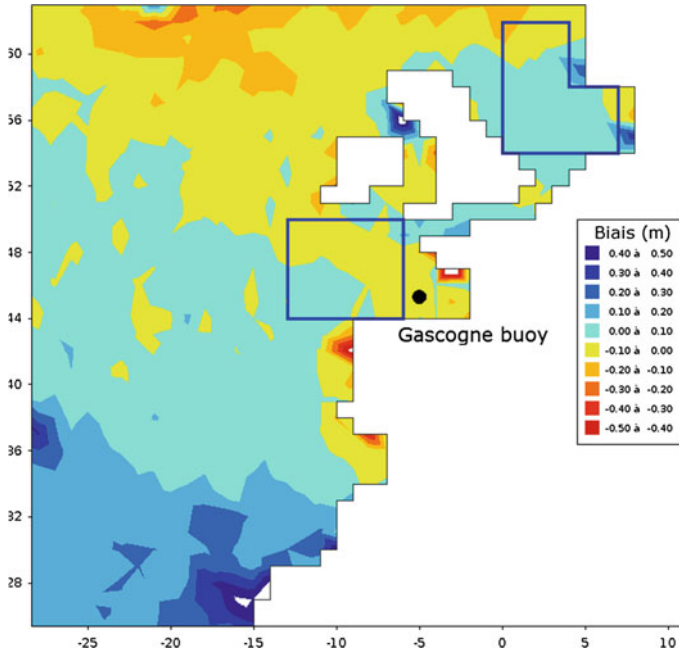


**Fig. 6** Spatial repartition of the bias (m) between  $H_{m0}$  from ANEMOC-2 and GlobWave altimeters over the period 2007–2009 focusing on the Bay of Biscay and North Sea areas over a grid of  $1^\circ \times 1^\circ$  resolution. Black node locates of the Gascogne buoy

## 4.2 Validation of the Mediterranean Model

### 4.2.1 Buoy Data Used for the Validation

To validate the Mediterranean model, 23 buoys located in the west Mediterranean Sea have been used (see Fig. 7). Table 2 shows their period of measurement beginning in 1998, where dark colors represent an annual temporal coverage greater than 50 %. Each color corresponds to the databases providing observations: Candhis and Météo-France along the French coast, RON (*Rete Ondametrica Nazionale*) along the Italian coast and XIOM (*Xarxa d'Instrumentacion Oceanografica I Meteorologica*) along the Spanish coast.

### 4.2.2 Statistical Parameter Calculated with Buoy Data

Table 3 shows the statistical parameters bias, RMSE, scatter index, and symmetric slope calculated over the period 2002–2008 with the available buoy data during this period. White cells correspond to the significant wave height  $H_{m0}$ , and gray ones to the mean period  $T_{02}$ .

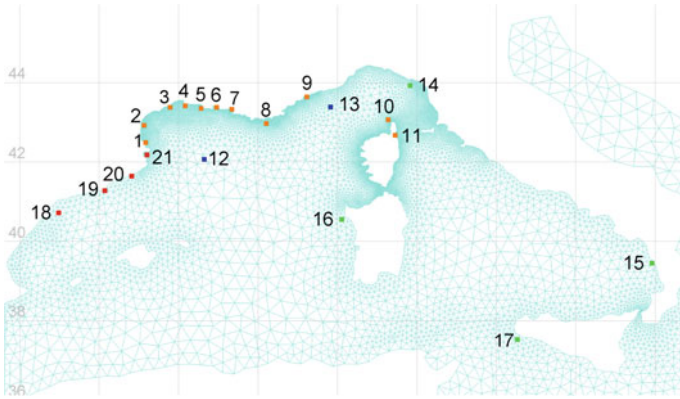


Fig. 7 Buoy location in the West Mediterranean Sea

Table 2 Temporal coverage of buoy measurements used for the validation step of the Mediterranean model of ANEMOC-2

Buoy	French buoys (candhis database)											Météo France buoys		Italian buoys				Spanish buoys					
	Banyuls	Lauvague	Sete Marsellian	Sete Frontignan	Sete	Espiguette	Camargue	Port de Bouc	Marseille	Porquerolles	Nice	Cap Corse	Bastia	Lyon	Cote d'azur	La Spezia	Cetraro	Alghero	Mazara	Tortosa	Llobregat	Blanes	Rosas
Buoy number	1	2	3	3	3	4	5	6	7	8	9	10	11	12	13	14	15	16	17	18	19	20	21
1998																							
1999																							
2000																							
2001																							
2002																							
2003																							
2004																							
2005																							
2006																							
2007																							
2008																							
2009																							

The bias between simulations and buoy measurements is low for the significant wave height, except on Porquerolles, Nice, and Cap Corse buoys, for which the bias is negative and quite important (between  $-13$  and  $-41$  cm). Apart from these three buoys, the accuracy of simulation results is homogeneous. Bias is almost always negative on buoys. RMSE shows errors between 3 and 8 cm for coastal buoys, which is satisfactory. Scatter index is about 30 to 40 %. Symmetric slope is often equal or lower than 1, which reflects the underestimation trend of the database on the buoys.

**Table 3** Statistical parameters between simulations results and in situ observations over the period 2002–2008

Buoys/Statistic indices		Bias		RMSE		Scatter index		Symmetric slope	
		$H_{m0}$ (cm)	$T_{02}$ (s)	$H_{m0}$ (cm)	$T_{02}$ (s)	$H_{m0}$ (%)	$T_{02}$ (%)	$H_{m0}$	$T_{02}$
Offshore buoys	Lion	5	-1.4	22	1.1	25	31	1.1	0.7
	Azur	-4	-1.8	11	2.5	28	43	1.0	0.7
French buoys (Candhis database)	Banuyls	-9	-0.8	7	0.5	31	26	1.0	0.9
	Leucate	-13	-0.6	7	0.9	36	30	0.9	0.9
	Sète	-9	-0.6	5	0.6	30	27	0.9	0.9
	Sète Frontignan	-9	-1.0	4	1.2	30	36	0.9	0.8
	Espiguette	-11	-0.6	8	0.8	29	27	1.0	0.9
	Camargue	-5	-0.7	5	0.4	28	24	1.0	0.8
	Port-de-Bouc	1	-0.7	3	0.5	26	27	1.1	0.8
	Marseille	-6	-1.1	7	0.9	41	36	0.9	0.7
	Porquerolles	-41	-0.8	26	0.4	39	22	0.7	0.8
	Nice	-13	-1.2	5	0.7	37	33	0.8	0.8
	Cap Corse	-19	-0.6	24	0.7	30	21	0.9	0.9
Bastia	-8	-1.0	3	0.4	37	30	0.9	0.8	
Italian buoys (RON database)	Alghero	-3	-0.8	8	2.0	20	32	1.0	0.8
	Cetraro	1	-1.1	6	3.4	26	43	1.0	0.7
	La Spezia	-13	-0.5	6	1.5	28	30	0.9	0.9
	Mazara	1	-0.7	7	1.0	20	26	1.0	0.9

We can notice that the statistical parameters highlight better simulations of the significant wave height than the mean period. As example, the negative bias between  $T_{02}$  simulations and observations is approximately  $-1$  s for the coastal buoys, and reaches  $-1.8$  s for the offshore buoys.

### 4.2.3 Scatter Plot for the Comparison with Buoy Data

Figure 8 shows scatter plots for the simulation wave height  $H_{m0}$  and data of Banyuls, Camargue, Nice and Azur buoys.

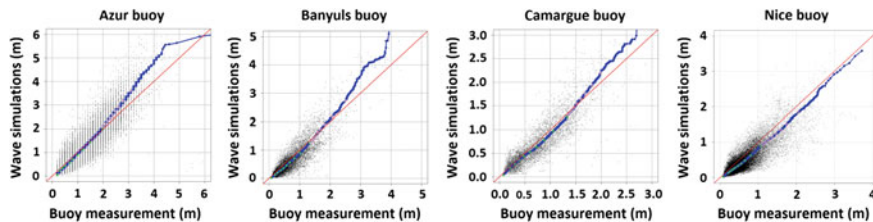


**Fig. 8** Scatter plots between wave height  $H_{m0}$  simulations and measurements of offshore and coastal buoys over the period 2002–2008 (see temporal coverage of buoy measurements Table 2)

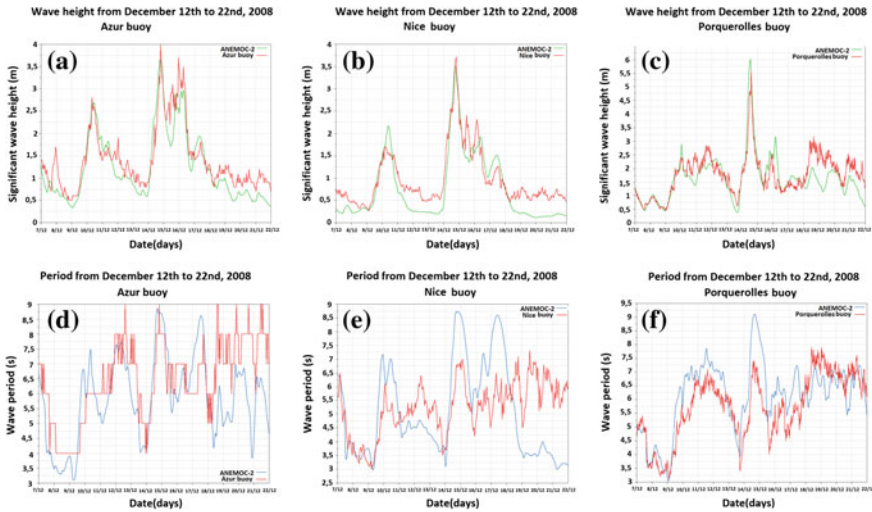


**Fig. 9** Comparison of ANEMOC-2 results and in situ observations during the storm from 7th to 22nd of December, 2008. Configurations **a**, **b**, and **c** correspond to  $H_{m0}$  at Azur, Nice, and Porquerolles buoys, respectively, and configurations **d**, **e**, and **f** correspond to  $T_{02}$  at Azur, Nice and Porquerolles buoys, respectively

For the three buoys Camargue, Banyuls, and Azur, even if the global bias is slightly negative, the tail of the distribution (for the wave height higher than the 90th percentile for Azur, and than the 95th percentile for the two others) is overestimated. On the contrary, Nice buoy tends to underestimate the whole distribution. On this buoy, simulations seem to show a constant bias for all the wave height.

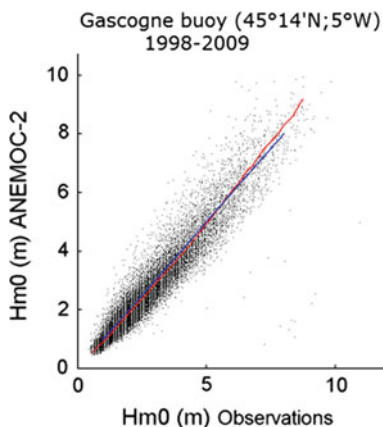
#### 4.2.4 Study of a Storm Event: From 7th to 22nd of December, 2008

Figure 9 compares significant wave height  $H_{m0}$  and mean period  $T_{02}$  calculated by the wave model and measured by the offshore buoy Azur (−2430 m), and the two coastal buoys Nice (−270 m) and Porquerolles (−90 m)—see location Fig. 7. Figure 9 a–c compare the  $H_{m0}$  for ANEMOC-2 and in situ observations, and Fig. 9d–f compare  $T_{02}$ . Figure 9a and d represents Azur buoy, 9b, e represent Nice buoy and 9c, f represent Porquerolles buoy.

In offshore and coastal areas, a good agreement is observed between ANEMOC-2 and buoys measurements for both  $H_{m0}$  and  $T_{02}$ . During this storm, peaks of  $H_{m0}$  coincide with peaks measured by the buoys. We can notice a slightly underestimation of the simulations after the peak of the event.

Variations of wave period are also well simulated on the three buoys. However, at the end of the event, the model underestimates the period on Azur and Nice buoys (~2 s). Near the coast, for Nice and Porquerolles buoys, period is overestimated at the peaks of the event (~2 s).

**Fig. 10** Quantile-quantile diagram of ANEMOC-2  $H_{m0}$  (m) and Gascogne buoy observations built over the period 1998–2009



### 4.3 Validation of the Atlantic Model

#### 4.3.1 Comparison with Buoy Data

Météo-France and Candhis buoys have been used to validate the oceanic and coastal models over the period 1996–2009. As example, the quantile-quantile diagram (Fig. 10) of the  $H_{m0}$  at the Gascogne buoy (see location Fig. 6) indicates the good correspondence between simulations and in situ observations until 7 m, then ANEMOC-2 tends to overestimate the highest value of  $H_{m0}$ .

At coastal locations, the validation step informs about the good reproduction of the  $H_{m0}$  and the mean period  $T_{02}$  along the Atlantic shoreline, while results slightly degrade along the English Channel and North Sea where wave-current interactions should be taken into account as tidal effects are significant in these areas.

#### 4.3.2 Study of a Storm Event: From 6th to 16th of February, 2009

The night between 9th and 10th of February 2009, the storm Quinten hit the Atlantic French coast with strong winds reaching 140 km/h at La Pointe du Raz (Brittany). Figure 11 shows the ability of the ANEMOC-2 significant wave height  $H_{m0}$  and mean period  $T_{02}$  to reproduce the wave climate during this extreme event at two locations: the Gascogne buoy (−4500 m, see location Fig. 6) and the Cap Ferret buoy (−54 m, see location Fig. 2c). Configurations Fig. 11a, b compare the  $H_{m0}$  of ANEMOC-2 and in situ observations in both offshore and coastal areas. In addition, configurations Fig. 11c, d compare the  $T_{02}$  between simulations and observations for both locations.

A general good agreement can be found between ANEMOC-2 and observations for  $H_{m0}$  and  $T_{02}$  in oceanic and coastal areas. Between 6th and 16th of February 2014, in situ observations characterized the storm Quinten by two peaks of  $H_{m0}$ .

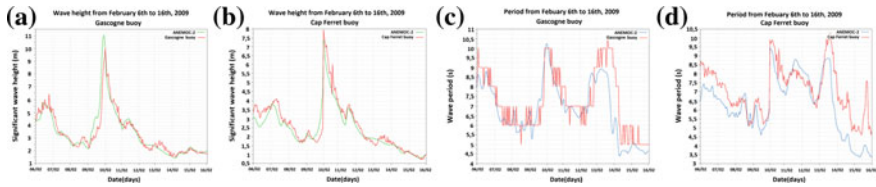


**Fig. 11** Comparison of ANEMOC-2 results and in situ observations during the Quinten storm (6th to 16th of February 2009). Configurations **a** and **b** correspond to  $H_{m0}$  at Gascogne and Cap Ferret buoys, respectively and configurations **c** and **d** correspond to  $T_{02}$  at Gascogne buoy and Cap Ferret respectively

also well reproduced by ANEMOC-2. The highest of both peaks reaches a  $H_{m0}$  of about 10 m at the Gascogne buoy and up to 8 m at the Cap Ferret buoy. For this storm, it can be seen that ANEMOC-2 slightly overestimate the peak of  $H_{m0}$  ( $\sim 1$  m) at Gascogne buoy, and slightly underestimate it at the Cap Ferret buoy (0.60 m). In addition, mean period  $T_{02}$  from ANEMOC-2 reproduces quite well the variations of the observations, while its value slightly underestimates them ( $\sim 1$  s).

## 5 Conclusion

Two new numerical wave databases, called ANEMOC-2, have been built over the period 1979–2010 covering the Mediterranean Sea and the Atlantic Ocean, and focusing on the French coasts. They provide several wave parameters (significant wave height  $H_{m0}$ , mean period  $T_{02}$ , peak period  $T_p$ , mean direction  $\theta_m, \dots$ ) with a high spatial (800 m to 1 km along the French coasts) and temporal (1 h) resolution. The methodology developed to construct these databases has been explained, focusing on the Mediterranean model: parameterization of the TOMAWAC wave model, calibration and validation steps by means of altimetry and in situ observations, respectively. Their analyses provide an assessment of many characteristics of both databases. For example, in offshore areas, the comparison with altimeter wave heights shows that the absolute value of the bias is lower than 10 cm over large areas. This bias also informs that in the Bay of Biscay and in the eastern part of Corsica, ANEMOC-2 slightly underestimates mean values of  $H_{m0}$ , while the wave atlases slightly overestimates them in the south of France and North Sea areas. In addition, the validation step shows that the bias on the Mediterranean coastal buoys is almost always negative, while it remains acceptable with a bias lower than 10 cm for most of cases.

Furthermore, ANEMOC-2 ability to reproduce extreme wave climate has been highlighted by analysis of two particular storm. For five locations, numerical simulations and in situ observations of  $H_{m0}$  and  $T_{02}$  have been compared. On the one hand, the study of Quinten storm peak shows that the Atlantic model tends to overestimates highest values of  $H_{m0}$  at some places, as seen at the Gascogne buoy for instance, while it also appears to slightly underestimate the  $H_{m0}$  highest value at



other places, as seen on the coastal Cap Ferret buoy. On the other hand, the study has shown that the Mediterranean model slightly overestimates the highest  $H_{m0}$  even in areas where the mean values of  $H_{m0}$  are slightly underestimated. Therefore it will not cause any underestimation of  $H_{m0}$  highest values, which is a highly valuable characteristic.

Finally, ANEMOC-2 databases will benefit from future improvements. For example, wave-current interactions will be taken into account in the coastal model around the Atlantic, English Channel, and North Sea French coast where tidal effects are important. The spectral decomposition will also be applied to better separate and characterize the wind sea and swell components. Lastly, ANEMOC-2 databases will be updated by means of CFSRv2 reanalysis for the years 2011 and following ones.

**Acknowledgements** The authors thank the NOAA for the provision of the CFSR reanalysis used in this work. Institutes IFREMER, Météo-France, CEREMA, ISPRA (RON), XIOM, LEGOS, and GEBCO are thanked, respectively for altimeter and scatterometer observations, in situ observations and bathymetric databases.

## References

1. Benoit, M., Marcos, F., & Becq, F. (1996). Development of a third generation shallow-water wave model with unstructured spatial meshing. *Proceedings of 25th Conference on Coastal Engineering*, Orlando (FL, USA), ASCE, pp. 465–478.
2. Benoit, M., & Lafon, F. (2004). A nearshore wave atlas along the coasts of France based on the numerical modelling of wave climate over 25 years. *Proceedings of 29th Conference on Coastal Engineering (ICCE'2004)*, Lisbonne (Portugal), pp. 714–726.
3. Benoit, M., Lafon, F., & Goasguen, G. (2008). Constitution et exploitation d'une base de données d'états de mer le long des côtes françaises par simulation numérique sur 23 ans. Base ANEMOC en Atlantique—Manche—Mer du Nord. *European Journal of Environmental and Civil Engineering*, 12(1–2), 35–50.
4. Bidlot, J.-R., Janssen, P. A. E. M., & Abdalla, S. (2007). A revised formulation of ocean wave dissipation and its model impact. ECMWF Tech. Rep. Memo. Reading.
5. Charles, E., Idier, D., Thiebot, J., le Cozannet, G., Pedreros, R., Arduin, F. et al. (2012). Present wave climate in the Bay of Biscay: Spatiotemporal Variability and trends from 1958 to 2001. *Journal of Climate*, 25, 2020–2039. doi:10.1175/JCLI-D-11-00086.1.
6. Dodet, G., Bertin, X., & Taborda, R. (2010). Wave climate variability in the North-East Atlantic Ocean over the last six decades. *Ocean Modelling*, 31, 120–131.
7. Hasselmann, K. et al. (1973). Measurements of wind-wave growth and swell decay during the Joint North Sea Wave Project (JONSWAP). *Deutschen Hydrographischen Zeitschrift*.
8. Hasselmann, S., & Hasselmann, K. (1985). Computations and parameterizations of the nonlinear energy transfer in gravity-wave spectrum. Part I: a new method for efficient computations of the exact nonlinear transfer integral. *Journal of Physical Oceanography*, 15, 1369–1377.
9. Janssen, P. (1989). Wave induced stress and the drag of air flow sea waves. *Journal of Physical Oceanography*, 19, 745–754.
10. Janssen, P. (1991). Quasi-linear theory of wind-wave generation applied to wave forecasting. *Journal of Physical Oceanography*, 21, 1631–1642.

11. Komen, G. J., Hasselmann, S., & Hasselmann, K. (1984). On the existence of a fully developed wind-sea spectrum. *Journal of Physical Oceanography*, *14*, 1271–1285.
12. Morellato, D., & Benoit, M. (2009). Construction d'une base de données d'états de mer le long des côtes françaises méditerranéennes par simulations rétrospectives couvrant la période 1979–2008. Colloque CM2, Tunis, décembre 2009.
13. Morellato, D., & Benoit, M. (2010). Constitution of a numerical wave data-base along the French Mediterranean coasts through hindcast simulations over 1979–2008. Colloque AIPCN MMX Congress 2010, Liverpool, Mai 2010.
14. Queffeuilou, P., & Croize-Fillon, D. (2009). La mesure satellite de hauteur de vague par altimètre. Etat des lieux, application à la climatologie et à la modélisation des états de mer. *Proc. AMA 2009. Les Ateliers de Modélisation de l'Atmosphère*, Toulouse.
15. Saha, S., et al. (2010). The NCEP climate forecast system reanalysis. *Bulletin of the American Meteorological Society*, *91*, 1015–1057.
16. Thornton, E. B., & Guza, R. T. (1983). Transformation of wave height distribution. *Journal of Geophysical Research*, *88*, 5925–5938.